Law *et al. Journal of Nanobiotechnology* (2025) 23:367
https://doi.org/10.1186/s12951-025-03459-y

Journal of Nanobiotechnology

RESEARCH Open Access

Harnessing intracellular bacteria in bladder by intravesical delivery of antibiotics-loaded nanodiamonds to reduce the recurrence of urinary tract infection

Carmen Oi Kwan Law[1†], Hoi Man Leung[2,3†], Meijun Wang[1†], Qichang Nie[1], Quynh Hoa Pham[1], Kam Chu Han[4], Tak Siu Wong[4], Kwan Ting Chow[1*], Pik Kwan Lo[2,3*] and Terrence Chi Kong Lau[1*]

Abstract

Treating urinary tract infections (UTIs) effectively is a difficult task due to the emergence of antibiotic-resistant bacteria and limited antibiotic access to intracellular bacteria within the bladder lining. Numerous studies of the antibiotics-nanodiamonds (NDs) synthesis and their inhibitory effect on bacteria have been performed previously. However, their effectiveness and toxicity in cell-based and animal infection models remain unclear. In this study, we presented the utilization of biopolymer-coated nanodiamonds for the delivery of tetracycline (TET) to the intracellular bacterial communities within the bladder cells using an intravesical delivery approach, aiming to effectively treat UTIs. Compared with antibiotics alone, the TET-loaded ND-based carrier system significantly improved the clearance of intracellular bacteria in the infected cell and animal models. Moreover, the intravesical delivery avoids the potential toxic effects from NDs accumulation in the organs, and minimizes the loss of the drugs during delivery. These results offer a promising strategy to treat chronic infections and prevent the recurrence of urinary tract infections (rUTIs).

†Carmen Oi Kwan Law, Hoi Man Leung and Meijun Wang contributed equally to this work and share the first authorship.

*Correspondence:
Kwan Ting Chow
kwan.chow@cityu.edu.hk
Pik Kwan Lo
peggylo@cityu.edu.hk
Terrence Chi Kong Lau
chiklau@cityu.edu.hk

Full list of author information is available at the end of the article

Graphical Abstract

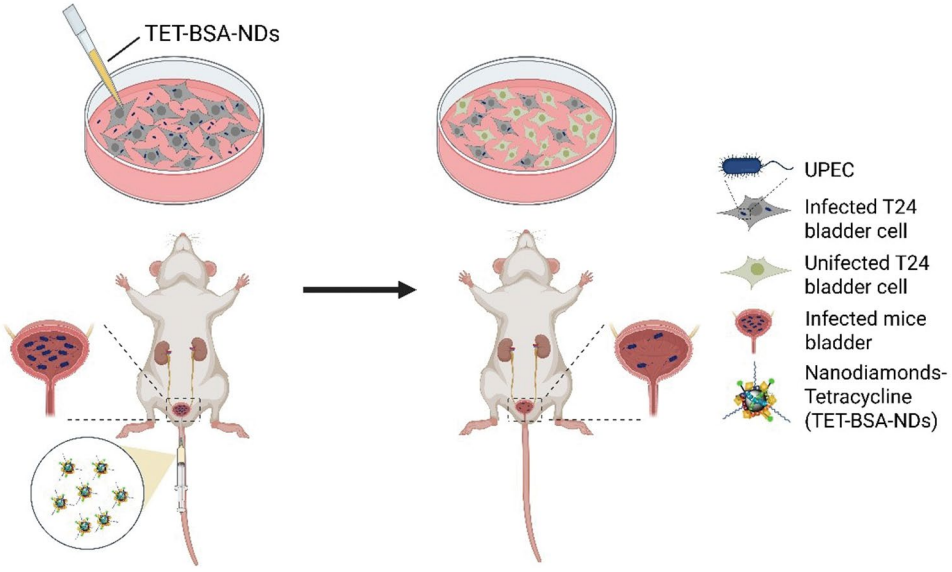

Keywords Antibacterial therapy, Antibiotics, Intravesical delivery, Nanodiamonds, Urinary tract infections

Introduction

Urinary tract infections (UTIs) are the second most common infection worldwide [1, 2], with an estimation of 400 million global cases per year [3] (more than 404.6 million in 2019; 95% UI 359.4-446.5 [4]), resulting in a total expense of six billion dollars in healthcare of the United States [5] and United Kingdom [6]. Nowadays, antibiotics remain the mainstay of the patient treatment, although the vaccine for UTI has been recently developed. However, the clinical values of conventional antibiotics have been alleviated dramatically because of the emergence of drug-resistant bacteria. Moreover, the poor accessibility of the drugs to the intracellular bacteria and the recurrence of UTI further enhance the difficulty of the treatment [7].

Uropathogenic *Escherichia coli* (UPEC) is the predominant causative agent that accounts for approximately 80% of UTIs [8]. It encodes a number of virulence factors that are responsible for the establishment of infection in the urinary tract. The internalized UPEC can rapidly proliferate within the cells to form transient biofilm-like intracellular bacterial communities (IBCs) or enter a quiescent state in which they form quiescent intracellular reservoirs (QIRs) for later re-emergence [9–11]. These subcellular structures of bacteria in umbrella cells can provide a shelter to protect the internalized UPEC from bladder immune response, such as the phagocytic activity by neutrophils and macrophages. Moreover, the subtherapeutic concentration in the cell due to the low penetrating power of the drugs reduces the efficiency of the antibiotic treatment and the clearance of intracellular UPEC, resulting in the promotion of recurrent UTI (rUTI) as well as the emergence of antibiotic resistance [9, 12]. Nowadays, the gold standard preventative treatment for rUTI in adult women is the continuous long-term low-dose antimicrobial therapy [13]. This antibiotic prophylaxis, according to a meta-analysis conducted by the Cochrane Collaboration, could effectively reduce up to 80% of rUTIs [14]. However, the prolonged subtherapeutic exposure often results in the development of antimicrobial resistance of causative bacteria or commensal flora [13, 15], making it difficult to be used as a common practice in clinical treatment.

Over the past few decades, nanotechnology has made significant advancements in the field of medicine [16–19]. Nanoparticles have been extensively utilized in the development of nanomedicines and delivery systems for therapeutic purposes, including tumor destruction [20], pathogen detection [21], and gene therapy [22–24]. In the case of treating UTIs, nanoparticle-based therapeutics offer a promising strategy to target drug-resistant bacteria [25, 26]. By improving drug solubility and cellular uptake [27, 28], nanoparticles have the potential to enhance the effectiveness of antimicrobial treatments and show antibacterial activity against various types of bacteria, including most Gram -positive and -negative bacteria and some drug-resistant strains of bacteria [29, 30]. For example, Malarkodi et al. utilized copper sulfide nanoparticles as an antibacterial agent to treat UTI in vitro caused by *E. coli*, *K. pneumoniae*, *P. vulgaris*,

and *S. aureus* [31]. The group of Padhy determined the antibacterial properties of silver nanoparticles to eleven uropathogens isolated from UTI patients [32]. The work of Ahmad et al. discovered that biogenic zinc oxide nanoparticles synthesized from *Mentha piperata* could effectively suppress the growth of multi-drug resistant strains of *Proteus mirabilis* and *Pseudomonas aeruginosa* isolated from UTI patients [33]. Despite the significant and promising results obtained from these studies, the clinical applications of nanoparticles are hindered by their potential toxicity [34]. For instance, silver nanoparticles release toxic ions that can damage cellular components and induce apoptosis [35], showing toxicity toward mammalian cell lines [36] and zebrafish embryos [37]. Similarly, zinc oxide nanoparticles cause pulmonary toxicity and oxidative stress [38]. These studies highlighted the adverse effects of metal-based nanoparticles on living organisms, emphasizing the importance of investigating options with reduced cytotoxicity for antibacterial therapy.

Nanodiamonds (NDs) have recently gained increasing interest as a theranostic tool in antibacterial therapy because of their chemical inertness, diverse surface functionalization, minimal cytotoxicity in mammalian cells and animals, and high loading capacity of antibiotics through physical adsorption [39, 40]. Bare NDs possess natural antibacterial properties, effectively eliminating both Gram -positive and -negative bacteria by using reactive acid anhydride groups on ND's surface [41]. Additionally, fully oxidized NDs can reduce intracellular bacteria without harming T24 bladder cells [42]. However, the antibacterial activity of bare NDs is only achievable at high concentrations, particularly in conditions free of proteins or media. Indeed, various strategies have been explored to enhance the antimicrobial properties of NDs including active molecules or antibiotics incorporation. For example, the surface of NDs can be complexed with amikacin/levofloxacin [39] or conjugated with mannose [43] or menthol [44] to inhibit biofilm formation, substantially improved the antimicrobial activity of NDs against *Escherichia coli* (*E. coli*) and/or *Staphylococcus aureus* (*S. aureus*). Rouhani et al. developed a targeted drug delivery system by loading amoxicillin onto polyethyleneimine-functionalized ferromagnetic material-based ND [45] and demonstrated the effective release of the drug at specific sites for the treatment of UTIs. Ho's group also incorporated amoxicillin-ND complexes into gutta-percha for bacterial eradication during root canal therapy [46], showcasing the biocompatibility and safety of NDs [47]. These findings demonstrated the high potential of NDs complexed with antibiotics as a potential antibacterial treatment in clinical applications.

Here, we developed an ND-based delivery system carrying antibiotic tetracycline (TET) for UTI treatment. We constructed the biocompatible TET-loaded bovine serum albumin (BSA) coated-NDs (TET-BSA-NDs) and investigated the therapeutic potency as the intracellular antibacterial drug in both UPEC-infected T24 bladder cells and UTI mouse models. The TET-BSA-NDs possessed high colloidal stability in different pH buffer systems, which are beneficial for improving drug delivery efficiency and therapeutic outcomes [48, 49]. Moreover, TET-BSA-NDs showed better and significant bactericidal effects on the intracellular bacteria in both in vitro and in vivo models when compared with the equivalent concentration of either TET or NDs alone. Besides, the cellular viability of infected cells after the treatment of TET-BSA-NDs was significantly improved, indicating the therapeutic potential of our ND-based delivery system. In addition, we adapted the procedure of intravesical administration that is often utilized in bladder cancer patients to deliver TET-BSA-NDs for the treatment of UTI in a mouse model, eliminating the potential accumulation of NDs in the liver, spleen, and lung. In summary, our study demonstrated how antibiotic-loaded nanodiamonds deliver and function in infected models and the potential usage of the intravesical delivery of antibiotic-functionalized NDs targeting IBCs for UTI therapy.

Results and discussion

Synthesis and characterization of TET-BSA-NDs

The problem of aggregation in physiological buffers hinders the loading and delivery efficiency of currently available NDs [49], leading to misinterpreted antibacterial effects [50]. Achieving monodispersity is crucial for using NDs as antibacterial carriers. As BSA has been identified as an excellent stabilizer against ND aggregation [51, 52], we have successfully developed an ND system coated with a layer of a BSA-derived biopolymer, not only facilitating efficient drug loading but also demonstrating high colloidal stability in various buffers [53]. The BSA-derived biopolymer (cBSA-PEG) was synthesized by covalently conjugating BSA with ethylenediamine and polyethylene glycol (PEG) chains as shown in Scheme 1. Under our reported reaction conditions [53], ~ 48 ethylenediamine molecules were attached to each BSA molecule, which was characterized by the mass difference between raw BSA and cBSA *via* matrix-assisted laser desorption ionization-time of flight (MALDI-TOF) mass spectroscopy studies (Figure S1-2). Subsequently, ~ 6 polyethylene glycol (PEG) chains with an average molecular weight of 5000 g/mol were successfully conjugated to the amino groups of cBSA to afford PEGylated cationized BSA (cBSA-PEG) *via* N-hydroxysuccinimide (NHS) chemistry (Figure S3). Additionally, we performed Fourier-transform infrared spectroscopy (FT-IR) to analyze the chemical composition of modified BSA and NDs. In the FT-IR spectra of proteins, raw BSA,

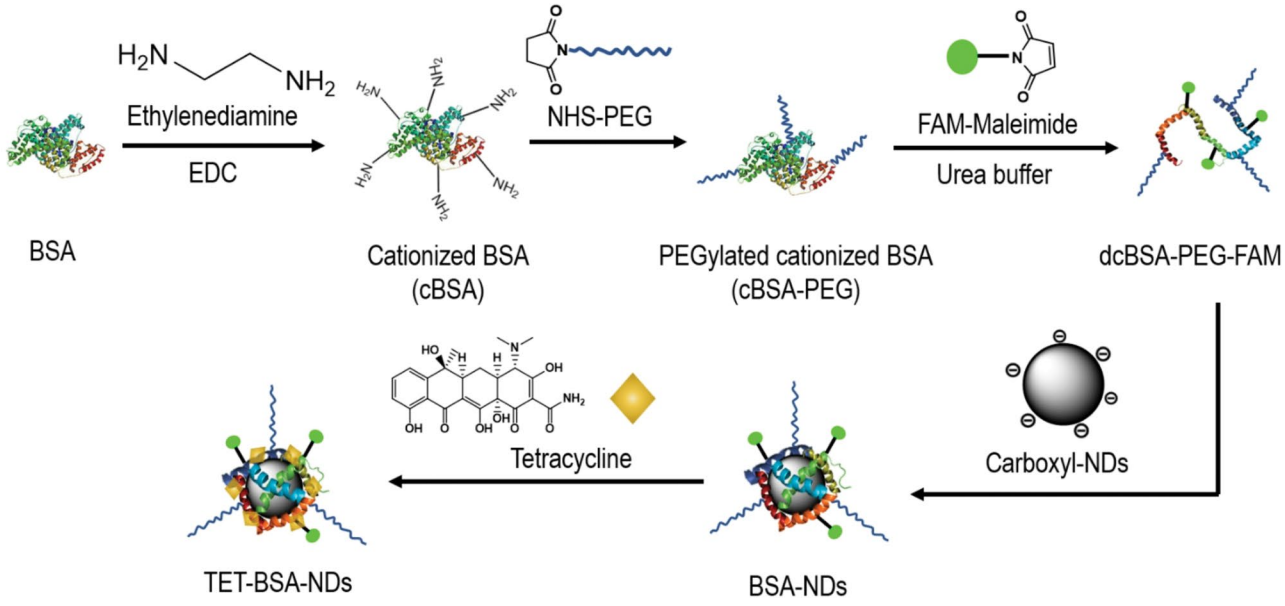

Scheme 1 Synthetic scheme of biopolymer-coated NDs loaded with tetracycline

cBSA, and cBSA-PEG exhibited characteristic absorbance at 1661 cm^{-1} and 1543 cm^{-1}, corresponding to amides I and II bands (Figure S4). The broad absorption peak at 3301 cm^{-1} indicated the stretching of O-H and N-H groups. Notably, the FT-IR spectrum of cBSA-PEG showed a significant increase in absorption at 2879 cm^{-1} and 1113 cm^{-1}, attributed to the stretching of C-H and C-O-C, respectively (red curve in Figure S4). This confirmed the successful conjugation of PEG chains to cBSA molecules. After denaturation, fluorescein (FAM) was attached through a thiol-maleimide reaction, resulting in dcBSA-PEG-FAM (Figure S5).

The carboxyl-NDs obtained after acid oxidation of raw NDs were then coated by stirring them in a solution of dcBSA-PEG-FAM. The resulting BSA-coated NDs (BSA-NDs) were purified and washed. Results of transmission electron microscopy (TEM) imaging revealed the change in agglomeration of NDs in the buffer after coating with the biopolymer. Uncoated carboxyl-NDs exhibited severe aggregation under 1X Phosphate buffered saline (PBS), while BSA-NDs still appeared in discrete particles (Fig. 1A). This confirmed that the coating of BSA-derived biopolymer was essential for maintaining the dispersity of NDs in physiological buffers. Dynamic light scattering (DLS) analysis results also showed an agreement with TEM imaging. The results from the DLS analysis presented in Fig. 1B and Table S1 demonstrate that the average size of the NDs increased from 43.47 ± 1.06 nm to 76.42 ± 4.32 nm in water after being coated with dcBSA-PEG-FAM. Additionally, the zeta potential increased from −70.5 ± 13.7 mV to -33.4 ± 2.2 mV, as shown in Fig. 1C. These findings confirm that the biopolymer coating provided protection to the NDs in Luria-Bertani (LB) medium. In contrast, carboxyl-NDs without the biopolymer coating formed micron-sized clusters (2.71 ± 0.69 μm) in LB medium, as indicated in Figure S6 and Table S1. We further characterized the modified NDs by FT-IR. In the FT-IR spectra of NDs (Fig. 1D), both raw NDs and carboxyl-NDs exhibited absorbance at 1792 cm^{-1}, corresponding to C = O vibration. The absorption peaks at 3438 cm^{-1} and 1633 cm^{-1} were assigned to O-H stretching and bending, respectively. The main feature in the FT-IR spectrum of carboxyl-NDs was the reduced intensity at 1095 cm^{-1}, indicating the removal of ether groups after acid oxidation. However, BSA-NDs showed higher absorption at 1111 cm^{-1} due to the presence of PEG from dcBSA-PEG coated on the surface. The FT-IR spectrum of TET-BSA-NDs exhibited a significant absorption peak of PEG at 1111 cm^{-1}, confirming the presence of dcBSA-PEG. On the other hand, a bicinchoninic acid (BCA) assay was used to quantify the amount of BSA coated onto the surface of NDs. Following the standard protocol of the BCA assay kit, the BSA functionalized on NDs was quantified with different amounts of NDs applied (31.25, 62.5, and 125 μg) based on the standard BSA calibration curve (Figure S7A). The protein quantification increased with the amount of NDs applied, and a linear correlation was observed with NDs under different dilutions (Fig. 1E and S7B). In contrast, negligible absorbance was detected in bare NDs, confirming that NDs had little interference with the protein determination. Through calculation, it was determined that 82.6 ± 6.9 μg of dcBSA-PEG was coated on 100 μg of NDs.

TET is known to exist as a zwitterion in neutral aqueous solution [54]. The protonated dimethylammonium

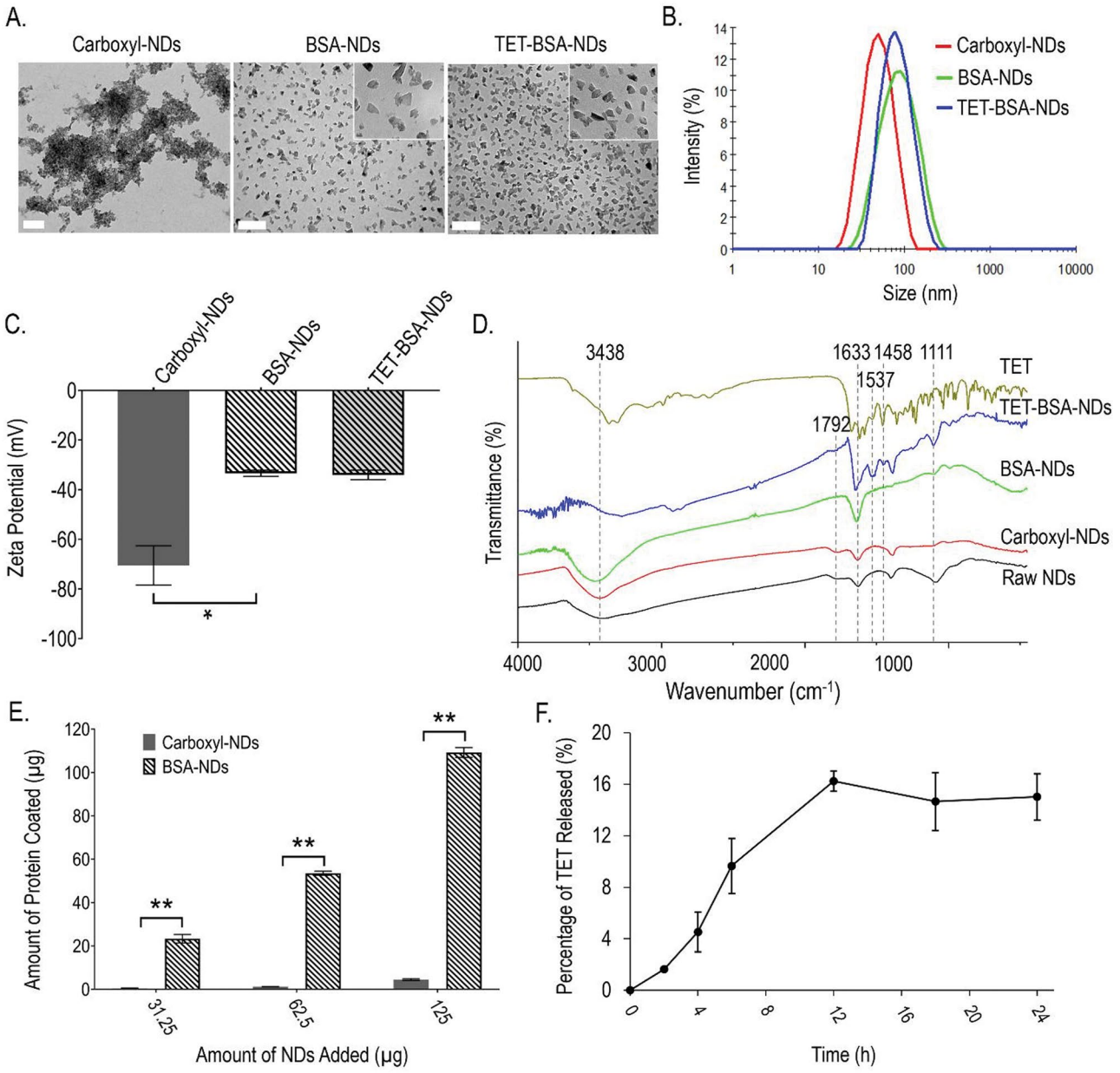

Fig. 1 Characterization of modified NDs. (**A**) TEM images of carboxyl-NDs, BSA-NDs and TET-BSA-NDs in 1X PBS, inset are the zoomed images of ND samples. The scale bars correspond to 200 nm. (**B**) Size distribution and (**C**) zeta potentials of carboxyl-NDs, BSA-NDs and TET-BSA-NDs in water. (**D**) FT-IR spectra of raw NDs, carboxyl-NDs, BSA-NDs, TET-BSA-NDs and TET. (**E**) Protein quantification of carboxyl-NDs and BSA-NDs by BCA assay. (**F**) Release kinetic of TET from BSA-NDs incubated in buffer with pH 6.0 at a concentration of 1 mg/mL for 0, 2, 4, 6, 12, 18 and 24 h. The release of TET over different time points was presented as a percentage relative to the amount of TET loaded onto the NDs. 1 mg/mL of TET-BSA-NDs was equivalent to 1.12 mg/mL of TET. Error bars in (**B**), (**E**) and (**F**) represent the mean ± standard error of the mean (SEM) of three independent experiments ($n = 3$). Data are analyzed using an unpaired t-test (two-tailed: *$p < 0.05$, ** $p < 0.01$, ***$p < 0.0001$)

group confers a positive charge, while the loss of proton from the phenolic diketone moiety results in a negative charge. This zwitterionic nature enables TET to engage in electrostatic interaction with charged amino groups present in BSA. The loading method of TET to BSA-NDs can be referred to our previous study with a comparable design [55], TET was physically adsorbed onto BSA-NDs by mixing them for 48 h. Excess TET was removed by centrifugation, and the resulting TET-BSA-NDs were washed with 1X PBS as shown in Scheme 1. TET typically displayed absorption peaks at 276 nm and 365 nm, as shown in Figure S8A. The concentration of TET remaining after the reaction was quantified by Ultraviolet–visible (UV-Vis) absorption, and the calibration curve was determined in Figure S8B. The quantification of unbound TET revealed that 0.42 ± 0.13 mg of TET was absorbed

onto 0.5 mg of BSA-NDs. The monodispersity and morphology of TET-BSA-NDs were similar to BSA-NDs in 1X PBS as shown in TEM imaging (Fig. 1A). According to DLS analysis, no significant differences were observed when comparing the size and zeta potential of TET-BSA-NDs with those of BSA-NDs in water (Fig. 1B and C). This suggests that the presence of TET did not affect the size or zeta potential of the NDs in the presence of the biopolymer coating. Furthermore, when examining the behavior of the NDs in LB medium, both the BSA-NDs and TET-BSA-NDs maintained similar sizes and displayed high monodispersity with a polydispersity index (PDI) of approximately 0.2 (Figure S6 and Table S1). FT-IR analysis revealed the successful adsorption of TET onto BSA-NDs. The FT-IR spectrum of TET-BSA-NDs showed a similar complexity to that of TET in the range of 450 cm^{-1} to 1800 cm^{-1}, with both exhibiting absorption peaks at 1458 cm^{-1} and 1537 cm^{-1}. These observations are in good agreement with the reported study [40]. Fluorescence analysis revealed that the emission of FAM in BSA-NDs was not altered after the immobilization of TET (Figure S9). To investigate the drug release capability of our ND system, we examined the release of TET from BSA-NDs by incubating them in buffers at different pH values. 1 mg/mL of TET-BSA-NDs in buffer solutions at pH 6.0, 7.4, and 8.0 were prepared and incubated at 37 °C for 24 h. The release of TET at pH 7.4 and 8.0, which represent the pH values of commonly used biologically relevant media, was very low, with release percentages of 2.3% and 2.6%, respectively (Figure S10). The release of TET in cell lysate was also low, approximately 2.5%, considering that the pH of the cytosol is known to be around 7.2. In contrast, the amount of TET released increased significantly, up to approximately 15.0%, when incubated in a buffer solution at pH 6.0. Furthermore, we observed that the release percentage increased with longer incubation time, reaching a plateau after 12 h (Fig. 1F). These results are consistent with a study conducted by Giammarco et al. [40], confirming that TET remains adsorbed to the NDs under conditions similar to biological media (e.g., slightly alkaline conditions), while the drugs dissociate from BSA-NDs under acidic conditions. This property prevents drug desorption before cellular internalization and allows release in slightly acidic organelles such as endosomes [56–58], which have pH values ranging from 5.5 to 6.5 [59]. In acidic conditions, the phenolic diketone group of TET undergoes protonation, leading to TET carrying a positive charge instead of its zwitterion form. Meanwhile, the carboxyl groups of amino acids within the BSA molecule also get protonated in an acidic environment. This protonation process diminishes the electrostatic interaction between BSA-NDs and TET, facilitating an acid-responsive release. Moreover, in comparison to the study by Giammarco et al., where less than 10% of TET was released from carboxyl-NDs at pH 4.09 over one-day incubation period, our BSA-NDs demonstrate exceptional carrier capabilities. Our BSA-NDs effectively protect against TET dissociation initially, and subsequently, approximately 25% of TET was released in a buffer system at pH 4.5 within a relatively short incubation time of 24 h (Figure S10).

Antibacterial effect of TET-BSA-NDs

To investigate the antibacterial effect of TET-BSA-NDs, we measured the minimum inhibitory concentrations (MIC) of TET-BSA-NDs and BSA-NDs against UPEC CFT073 [60, 61]. BSA-NDs were used as a control to rule out the potential intrinsic antibacterial properties of the nanocarrier itself. The bacteria were directly treated with the increasing concentrations of each compound in LB broth (pH 7.0), and the viability of bacteria was measured. As shown in Fig. 2A, the nanocarrier BSA-NDs did not exhibit any inhibitory effect in bacterial growth by itself. In contrast, 5 μg/mL of TET-BSA-NDs demonstrated a 30% reduction in the cell viability. Assuming that the bactericidal activity of TET-BSA-NDs was attributed to the released TET as the nanocarrier has no antibacterial effect (Fig. 2A), the effective concentration of TET to kill the bacteria should be equal to the concentration of released TET. Since the percentage of TET released from TET-BSA-NDs was 2.3% at pH 7.4 (Supplementary Figure S10B), the effective concentration of TET is $[TET_{release}] = 2.3\% \times [\text{TET-BSA-NDs}]$. To compare the antibacterial activity of TET-BSA-NDs with free TET, the effective concentrations of TET and the free TET was plotted against the viability of bacteria (Fig. 2B). The MIC of $TET_{release}$ and free TET was 0.8 μg/mL and 1.1 μg/mL respectively, suggesting the loading of TET into the ND nanocarrier did not reduce the antibacterial activity. Noteworthy, the amount of TET released increased significantly, up to approximately 15.0% and 25% under pH 6.0 and 4.5 respectively, which is similar to the conditions of endosome environments.

The bactericidal effects of TET-BSA-NDs on intracellular Bacteria of infected bladder cells

To evaluate the therapeutic potency of TET-functionalized NDs, cellular uptake and bactericidal effect on the intracellular bacteria were measured in CFT073-infected T24 bladder cells according to the study by Subramaniam et al. [62]. The UPEC strain CFT073 carrying mCherry fluorescent protein (CFT073-mCherry) was generated as the marker to identify the UPEC-infected host cells (Fig. 3A). TET-BSA-NDs were also labeled with FAM, which emits strong fluorescence at 520 nm, for tracing the localization of the NDs in the cells. BSA-NDs and TET were used as controls. To ensure that only intracellular bacteria were tested in our experiments, the infected

T24 bladder cells were first treated with gentamicin to eliminate all extracellular bacteria. They were then purified based on the mCherry fluorescent signal using a flow cytometer (Fig. 3A and S11). As shown in Fig. 3A, substantial amounts of TET-BSA-NDs were internalized into the bladder cells after the treatment of the infected T24 cells (green dot). Moreover, intriguingly, some TET-BSA-NDs even colocalized with the bacteria in the cytoplasm of the infected T24 bladder cells.

To assess the antibacterial activity of TET-BSA-NDs, the viability of intracellular bacteria in the infected cells was determined and compared with the control treatments (equivalent amounts of free TET and BSA-NDs). The colony-forming unit (CFU) was used to measure the bacterial viability in the cells after 24 h of treatment. As depicted in Fig. 3B, no significant difference between the control (no treatment) and TET-treated samples was observed, suggesting that the current dosage of TET is not enough to diffuse into the infected T24 cells. Conversely, treatment with TET-BSA-NDs significantly reduced the intracellular bacteria compared to the controls (approximately 60%.), indicating that BSA-NDs

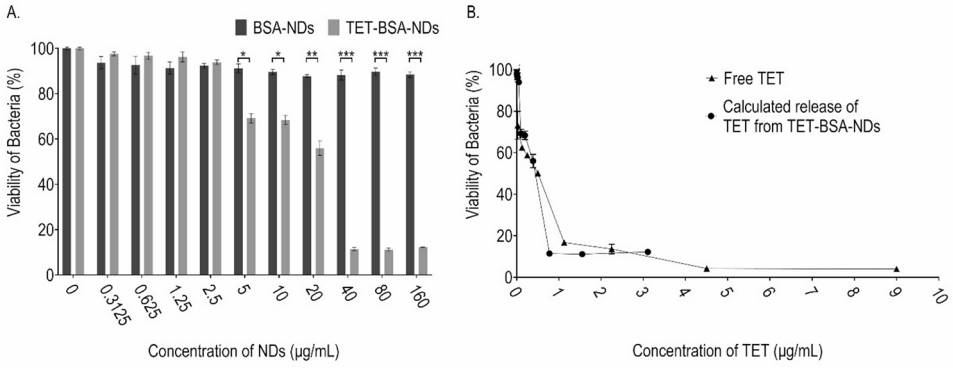

Fig. 2 Bactericidal effect of the BSA-NDs, TET-BSA-NDs and TET on uropathogenic *Escherichia coli* CFT073. The bacteria was treated with increasing concentrations of BSA-NDs, TET-BSA-NDs and Free TET overnight at 37 °C in LB broth at pH 7.0. The optical density at 600 nm (OD600), which represents the bacterial growth, was measured after incubation. The OD600 of the sample without any treatment was set as 100% viability. The results were expressed as the means of at least three independent experiments. Error bars present the mean ± SEM of at least three independent experiments ($n \geq 3$). Data are analyzed using an unpaired t-test (two-tailed: *$p < 0.05$, ** $p < 0.01$; ***$p < 0.0001$). (**A**) The percentage of bacterial viability was plotted against the concentration of NDs. (**B**) The percentage of bacterial viability was plotted against either the free TET or the calculated release of TET [$TET_{release}$] = 2.3% × [TET-BSA-NDs] where 2.3% is the experimentally pre-determined percentage value of TET release from TET-BSA-NDs at pH 7.4 (Figure S10)

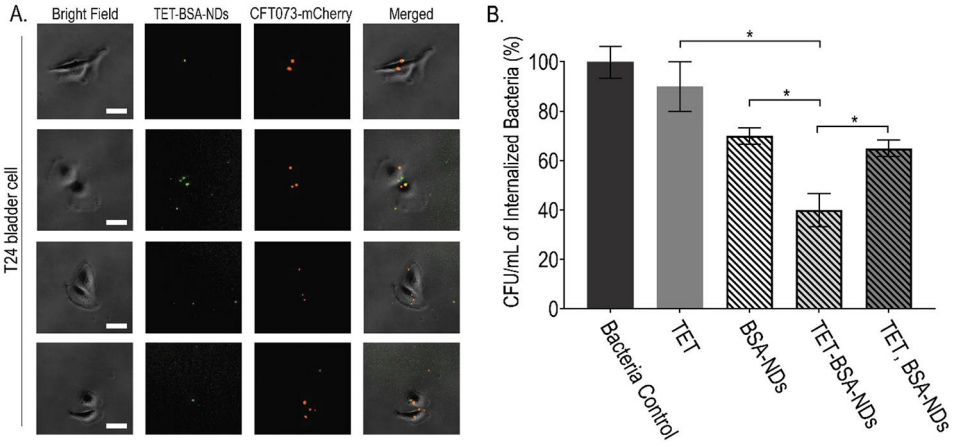

Fig. 3 Effect of the TET-BSA-NDs treatment in intracellular uropathogenic *Escherichia coli* CFT073. T24 bladder cells were incubated with CFT073-mCherry for 1 h. The cells were then washed with PBS and treated with 150 μg/mL of gentamicin for 1 h to kill extracellular bacteria, the *E. coli* mCherry + infected cells were sorted out and followed by incubation of 5 μg/mL of free TET, BSA-NDs only, TET-BSA-NDs and co-treatment of free TET with BSA-NDs for 24 h in a completed McCoy's 5 A medium modified with 10 μg/mL of gentamicin, respectively. 5 μg/mL of TET-BSA-NDs is equivalent to immobilized with 4.22 μg/mL of TET. (**A**) Immunofluorescence analyses characterizing the localization of FAM-labelled TET-BSA-NDs and CFT073-mCherry in T24 cells. TET-BSA-NDs and CFT073-mCherry (red) showed some of which colocalized each other in T24 bladder cells. The scale bars correspond to 25 μm. (**B**) The infected cells were lysis and intracellular CFT073-mCherry were enumerated after 24 h of treatment. The CFU count for the bacteria control sample was determined as 100%. The CFU count for the different treatment samples was normalized to the bacteria control sample. The result was expressed as the means of at least three independent experiments. Error bars present the mean ± SEM of three independent experiments ($n = 3$). Data are analyzed using an unpaired t-test (two-tailed: *$p < 0.05$, ** $p < 0.01$, ***$p < 0.0001$)

serve as an excellent carrier to deliver the drugs into cells efficiently and target the intracellular bacteria below the MIC of free TET (4.22 μg/mL). Moreover, when we compared individually the antibacterial effect of free BSA-NDs or free TET, we found that BSA-NDs contributed better in the clearance of intracellular bacteria than TET. Although the percentage release of TET from the ND carrier was determined to be 15% under acidic environments, the drug efficacy could still be significant, especially in scenarios where there are an average of 1 to 2 bacteria present within a T24 cell [63]. Since small sized-NDs have been reported to possess the bactericidal effect [41, 42], we also tested the antibacterial activity of BSA-NDs as well as the mixtures of TET and BSA-NDs to eliminate the possibility of additive effects. As shown in Fig. 3B, treatment with BSA-NDs or BSA-NDs/TET cannot provide the same or similar antibacterial activity as TET-BSA-NDs at the equivalent concentrations, indicating the potency of TET-BSA-NDs as the drug to deliver TET to target intracellular bacteria. Provided that the cytotoxicity of TET-BSA-NDs was very low (Figure S12), NDs serve as biocompatible tools for delivering therapeutic drugs to eliminate the intracellular bacteria of UTIs, potentially alleviating the recurrence of the infection.

Recurrence or the chronic nature of infections presents significant challenges in clinical treatment, largely due to the presence of IBC. Additionally, many antibiotics are not specially designed to penetrate cell membranes and are susceptible to degradation by enzymes in the cytosol [64–66]. High doses of antibiotics are often required to compensate for their low penetration power into cells to target these bacteria; however, this approach is accompanied by encountered toxicities, side effects, and the enhanced potential of developing antibiotic resistance [67–73]. Currently, there is no specific drug or molecule that effectively targets IBC. In our study, we focused on the formulation development of drugs to reach intracellular bacteria using a specific carrier which brings the antibiotics into the cells. TET is a broad-spectrum antibiotic active against a wide range of bacterial infections, such as acne, plague, UTIs, and other infections caused by susceptible Gram-negative bacteria [74]. A pilot clinical trial results supported that 66.7% (8 out of 12) hospitalized patients with UTIs were successfully treated with TET without regard to disk sensitivity. These findings suggested that TET may be an acceptable empiric approach to treating UTIs in non-septic hospitalized patients [75]. Besides, a comparative study by Rosenstock, J., et al. evaluated single-dose TET to conventional therapy of UTI. The result demonstrated that the cure rate by the treatment of single-dose TET (2 g), multi-dose TET (500 mg four times/ day, for 10 days), and single-dose amoxicillin (3 g) in women with UTIs were 75%, 94%, and 54%, respectively. This finding suggested that single-dose TET demonstrates comparable efficacy to other antibiotic regimens regardless of the susceptibility of the initial pathogen and has minimal toxicity. These promising results/ potential advantages warrant further investigation of TET as a single-dose therapy for uncomplicated UTIs [76]. While TET has shown therapeutic potential for UTIs, its poor urinary excretion limits its clinical utility as a first-line UTIs treatment [74, 77]. For this reason, our intravesical delivery approach may represent a promising solution that could overcome this pharmacological challenge (enhanced localized antibiotic concentration and improved intracellular penetration), potentially making TET a more effective option for chronic UTIs management and preventing rUTIs in the future.

While we have attempted to load other antibiotics, such as Fosfomycin, onto BSA-NDs carrier, their loading efficiency is inferior to that of TET (unpublished data). Also, the loading of Fosfomycin causes the aggregation of nanoparticles, which is not feasible for drug delivery. Nevertheless, our intravesical delivery approach, combined with the TET-BSA-NDs system, has demonstrated promising results against IBC in both in vivo infected T24 bladder cell models and mouse models. Although TET is not a first-line antibiotic treatment for UTIs and resistance remains a concern, this proof-of-concept study highlights the potential of our combined delivery strategy to deliver low concentrations of antibiotic(s) to enter the host cells and kill the intracellular bacteria. Importantly, the NDs platform can be adapted to carry other antibiotic(s) for against IBC treatment, though further optimization is needed.

Indeed, several studies suggested that TET synergy with other antibiotics could revitalize its clinical utility. A study investigated the synergistic effects of combining TET with other antibiotics against multidrug-resistant Gram-negative bacteria (*E.coli*, *Pseudomonas aeruginosa*, *Klebsiella pneumoniae* etc.) The results revealed that TET effectively synergized with various antibiotics, particularly ampicillin (AMP), cloxacillin (CLX), and chloramphenicol (CHL), at sub-inhibitory concentrations (MIC/5–MIC/10 of TET). This combination significantly reduced the minimum inhibitory concentration (MIC) up to 1024-fold compared to monotherapy. This study concluded that TET combined with other antibiotics could potentially restore antibiotic efficacy against multidrug-resistant Gram-negative bacteria strains [78]. Moreover, amoxicillin, a first-line antibiotic for treating urinary tract infections (UTIs), demonstrated strong synergy (87.5%) against various bacteria when combined with TET. These combinations were effective against Gram-negative and Gram-positive bacteria, including strains resistant to amoxicillin alone. This indicated that

TET-amoxicillin combination therapy may be far more effective than either antibiotic used alone [79].

For the purpose of proof-of-concept, TET-BSA-NDs which were utilized as carriers [67, 80, 81] to deliver low concentrations of antibiotics to enter the host cells and kill the intracellular bacteria. Based on the results of the release kinetics and colocalization test (Figs. 1F and 3A), there are two possible mechanisms that can describe the antibacterial functions of TET-BSA-NDs, (1) TET was released during the endosomal retention of TET-BSA-NDs after cellular uptake through clathrin-mediated endocytosis and micropinocytosis [82]. (2) The close contact of TET-BSA-NDs with bacteria also contributes to the release of TET and boosts antibiotic efficacy [83, 84]. Indeed, TET-BSA-NDs provide a more promising approach to treat chronic infections and prevent the recurrence of UTIs compared to other inorganic nanoparticles. For example, Rahuman et al. reported an antibacterial effect using silver nanoparticles capped with antimicrobial *C. carandas* leaf extract at a concentration of 40 µg/mL [85], while Ahmad et al. reported the antibacterial impact of *Mentha piperata*-derived zinc oxide nanoparticles at a minimum concentration of 25 µg/mL [33]. Our designed ND carrier has shown remarkable drug efficacy in UTI treatment at a low concentration applied.

Recovery of infected bladder cells by TET-BSA-NDs

Host cells act as a protective refuge to shield internalized UPEC from being attacked by the immune response. Moreover, the low penetrating power significantly reduces the effective concentration of the drugs, causing insufficient clearance of UPEC that leads to the failure of the medical treatment. The surviving bacteria will replicate inside the host cell and induce cell death by producing bacterial toxins or expressing virulence factors. The released bacteria from the death cells will re-enter infectious cycles and perpetuate the infection [9, 86–88]. We previously demonstrated that TET-BSA-NDs can enter the infected T24 cells and co-localize with the intracellular bacteria. To determine the therapeutic efficacy of TET-BSA-NDs, we examined the cell viability of the infected cells upon treatment. The bladder cells were first infected with the CFT073 bacteria, then underwent daily treatment with equivalent amounts of free TET, BSA-NDs or TET-BSA-NDs for the next four consecutive days (Fig. 4A i). A single dosage administered after 24 h of infection, followed by daily replacement with fresh medium, was also investigated (Fig. 4A ii). Infected cells incubated with a culture medium were only used as a control (bacteria control). As shown in Fig. 4B and C, both multiple dosages and single dosage of TET-BSA-NDs treatment improved cell viability by 2.5-fold and 2-fold, respectively, when compared to the bacteria control groups. These results suggested that no additional positive effect was achieved by multiple dosages. Noteworthy, an equivalent amount of TET only partially protected the infected cells. These results strongly suggest the significant role of NDs as efficient carriers to transport TET into cells, thereby achieving an effective concentration of antibiotics intracellularly to eliminate the bacteria inside the host cells, rescuing the bladder cells from apoptosis during UTI. On the other hand, free TET cannot efficiently penetrate into the host cells, resulting in the reduced effectiveness of the clearance of intracellular bacteria, increasing the risk of developing chronic infections.

Evaluation of antibacterial potency of TET-BSA-NDs in UTI mouse model

In vitro studies of TET-BSA-NDs demonstrated that NDs effectively brought the TET into the cells and killed the intracellular bacteria, improving the viability of the host cells. To further investigate the impact of TET-BSA-NDs on IBC proliferation and their effects on immune response in the bladder, a UTI mouse model was established. First, we induced UTI in C57BL6 mice by transurethral inoculation of CFT073-mCherry for 6 h, and then administrated the equivalent amount of TET, BSA-NDs or TET-BSA-NDs transurethrally. Infected mice treated with PBS were used as controls. Effective drug delivery remains a significant challenge in the therapeutic development of NDs, as they often accumulate in the liver, spleen, and lungs [89, 90]. To tackle this issue, we employed urethral catheterization as a delivery method for introducing the NDs directly to the bladder for UTI therapy. This approach has several advantages. Firstly, it extends the duration of NDs' presence in the bladder, enhancing their therapeutic potential. Secondly, it minimizes the toxic effects associated with off-target biodistribution in the host. This assumption is supported by a study conducted by Miao et al., where the distribution of nanoparticles in different organs was investigated post-intravesical delivery [91]. Their findings revealed a significant concentration of particles fluorescence signal in the bladder, with negligible presence in organs like the liver, kidney, and spleen. Additionally, this technique helps to mitigate possible losses during delivery, ensuring the maintenance of effective drug concentrations and achieving the desired therapeutic outcome. Consequently, this approach holds promise as a generic method for delivering NDs in future applications.

To monitor the infection within the mice's bladders in-situ, we captured images using an i imaging system (IVIS images) and compared the mCherry signal (as previously described) among treatment groups. The antibacterial effect of the NDs was determined before and after treatments. As shown in Fig. 5A ii, we found that the mice

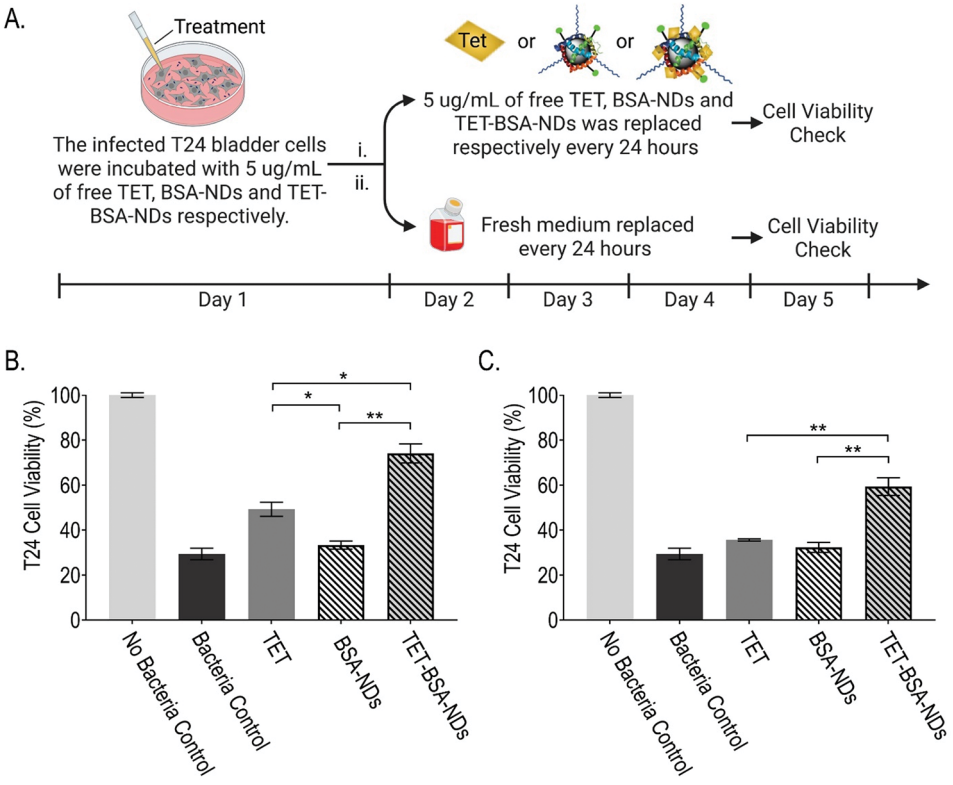

Fig. 4 Effect of the TET-BSA-NDs treatment in UPEC-infected T24 bladder cells. (**A**) Experimental timeline scheme for infected T24 bladder cells. T24 bladder cells were incubated with E. coli CFT073 for 2 h. The cells were then washed with PBS and treated with 150 µg/mL of gentamicin for 2 h to kill extracellular bacteria and then incubated with 5 µg/mL of fee TET, BSA-NDs only and TET-BSA-NDs in a completed McCoy's 5 A medium modified with 10 µg/mL of gentamicin, respectively. (i) & (**B**) Infected cells were received multiple doses of treatment in four consecutive days. (ii) & (**C**) Infected cells were received a single dose of treatment on Day 1 and followed by replaced medium daily for the next three days. 5 µg/mL of TET-BSA-NDs is equivalent to immobilized with 4.5 µg/mL of TET. No bacteria control and bacteria control served as negative and positive control, respectively. The cell viability for no bacteria control sample was determined as 100%, and all other samples were normalized to no bacteria control sample. The result was expressed as the means of at least three independent experiments. Error bars present the mean ± SEM of three independent experiments ($n = 3$). Data are analyzed using an unpaired t-test (two-tailed: $^{*}p < 0.05$, $^{**}p < 0.01$, $^{***}p < 0.0001$)

were able to naturally clear most bacteria in the urinary tract and bladders within one day after infection (bacterial control group). Moreover, treatments of neither TET nor BSA-NDs (Fig. 5A iii and iv) eradicated the intracellular bacteria (the IBC in the bladder cells). Intriguingly, on the other hand, TET-BSA-NDs can completely remove all the bacteria in the bladders of infected mice (Fig. 5A v), demonstrating its excellent antibacterial clearance for intracellular bacteria. The fluorescent signals were quantitated to evaluate the bactericidal effects of the compounds (Fig. 5B). Noteworthy, we observed swollen and inflamed bladders in all samples except the one treated with TET-BSA-NDs when compared to no bacteria control (Fig. 5C), suggesting the anti-inflammatory effect of TET-BSA-NDs.

Acute cystitis is a condition caused by excessive inflammation in the urinary bladder, resulting in symptoms such as pain, frequent urination and urgency [92]. Immune cells, such as neutrophils, monocytes and macrophages, are essential elements of the host innate immune response to UTIs. Macrophages and uroepithelial cells produce pro-inflammatory cytokines and chemokines during UTIs to recruit neutrophils to the infection site and modulate antimicrobial defenses. In Fig. 5D, qPCR analysis that the expressions of pro-inflammatory genes interleukin (IL) (IL-1β and IL-6), interferon signaling components (IFNAR and IFNβ), tissue remodeling enzymes (COX2 and MMP9), chemokines (CCL2, CCL5, CXCL9 and CXCL11), pathogen recognition receptors (TLR4), tumor necrosis factor α (TNF-α), and the neuropeptide substance P precursor (Pre-SP) in infected mice treated with PBS (bacteria control), TET and BSA-NDs were substantially elevated in bladder tissue, highlighting a robust macrophage-driven immune response. These genes are central to macrophage activation, cytokine production, leukocyte recruitment, and tissue inflammation [93, 94]. In contrast, the expression levels of IL-1β, IL-6, COX2, CCL5, CXCL9, CXCL11, TNF-α, TLR4, and Pre-SP were significantly lower in the bladder of TET-BSA-NDs-treated mice compared to other groups. Moreover,

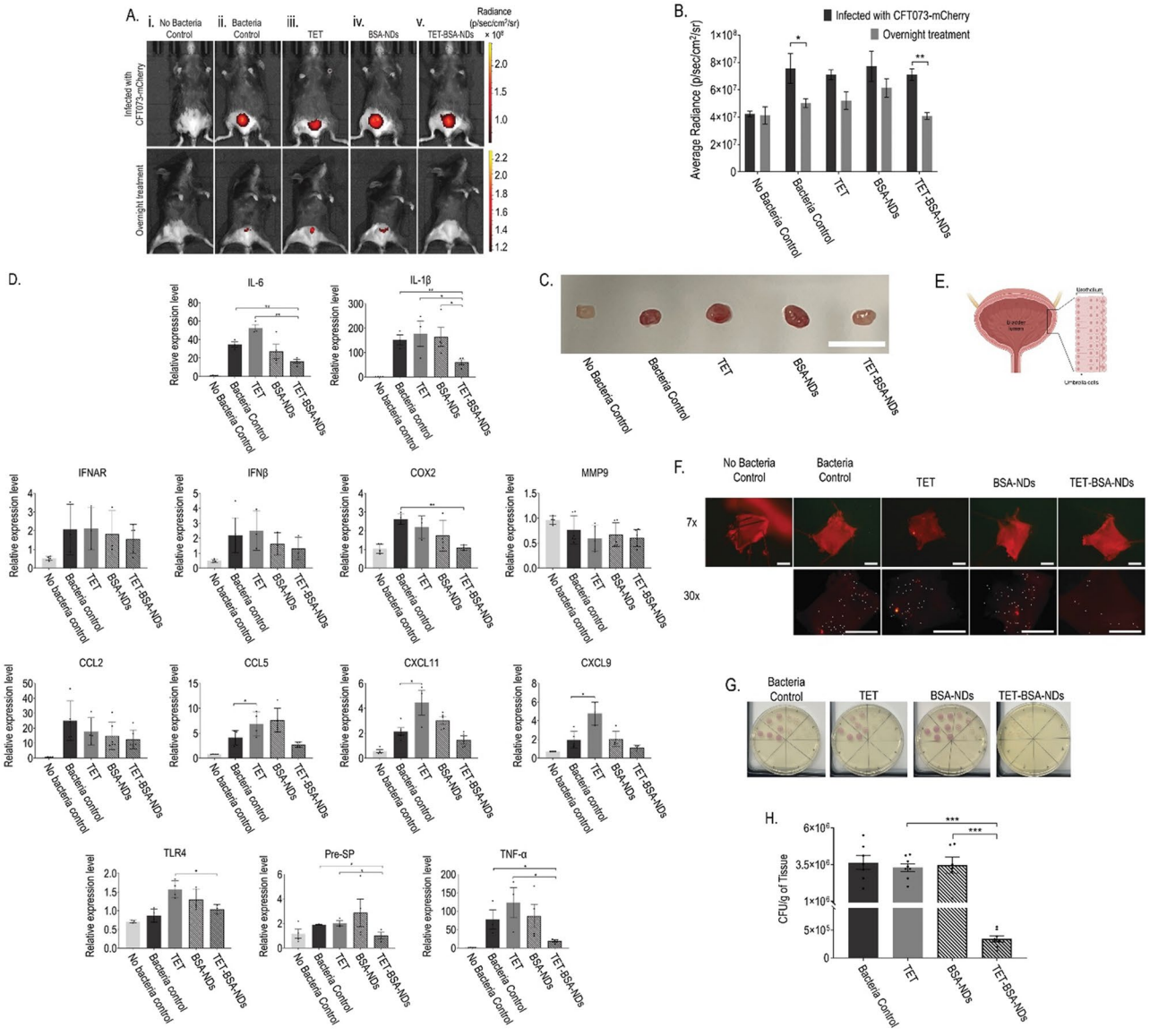

Fig. 5 Infection of C57BL6/J female mice with UPEC CFT073-mCherry. 7 weeks old C57BL6/J mice were transurethrally inoculated with 1×10^8 CFU CFT073-mCherry for 6 h. At 6 h post-infection, 5 µg/mL of free TET, BSA-NDs and TET-BSA-NDs was injected transurethrally into the bladder, respectively. PBS as bacteria control. 5 µg/mL of TET-BSA-NDs is equivalent to immobilized with 4.22 µg/mL of TET. After overnight, the bladder was harvested. (**A**) Representative images were obtained by In vivo Imaging System (IVIS) after being infected with UPEC CFT073-mCherry and after receiving overnight treatment. The pseudo-color scales indicated the radiant efficiency of each mouse. (**B**) Based on bacteria that expressed the fluorescence protein mCherry, the intensity of radiant efficiency emitted from each bladder of mice in (**A**) was quantified. $n = 3$ mice/ group. The experiment was performed with 3 mice for each group. Error bars present the mean ± SEM of three independent experiments ($n = 3$). (**C**) Representative photographs of normal and infected mice bladder with or without received treatment. The scale bar corresponds to 1 cm. (**D**) Analysis of interleukin (IL16 and IL-1β), interferon signaling components (IFNAR and IFNβ), tissue remodeling enzymes (COX2 and MMP9), chemokines (CCL2, CCL5, CXCL9 and CXCL11), pathogen recognition receptors (TLR4), tumor necrosis factor α (TNF-α), and the neuropeptide substance P precursor (Pre-SP) relative mRNA expression level using qPCR in response to different treatments for mice bladders. Error bars present the mean ± SEM of at least three independent experiments ($n \geq 3$). (**E**) Structure of the bladder and (**F**) The representative image displays a splayed bladder showing a mCherry red fluorescent protein-expressing IBCs (indicated by white arrows) under a motorized fluorescence stereoscope. The scale bars correspond to 2.5 mm. (**G**) Representative photographs of CFU counting of the bladder urothelium. CFUs of CFT073-mCherry dots on the LB agar plate containing kanamycin in a 10-fold dilution gradient. (**H**) After harvesting the bladder, open it and subsequent gentamicin treatment before homogenizing that allowed the enumeration of IBC only (bacteria in urothelium). The CFU count for the different treatment samples was normalized to the bacteria control sample. $n \geq 5$ mice/ group. The experiment was performed with at least 5 mice for each group. Error bars present the mean ± SEM of at least five independent experiments ($n \geq 5$). All data are analyzed using an unpaired t-test (two-tailed: $^*p < 0.05$, $^{**}p < 0.01$, $^{***}p < 0.0001$)

down-regulation was also observed for INFβ, IFNAR, MMP9, and CCL2 in the TET-BSA-NDs-treated mice group. Macrophages are pivotal in detecting pathogens via TLR4, which triggers NF-κB signaling and subsequent cytokine release (TNFα, IL-1β, IL-6) [93, 95]. Elevated COX2 and MMP9 indicate prostaglandin-driven inflammation and tissue damage, while chemokines like CCL2 and CXCL9 recruit monocytes and T cells [95–98]. The upregulation of these genes in infection aligns with expected macrophage responses. IL-1β plays a crucial role in mediating the inflammatory response and influencing various cellular activities, such as proliferation, differentiation, and apoptosis. In the clinic, patients with bacterial cystitis often display elevated levels of urinary interleukin IL-1β compared to individuals with Interstitial Cystitis/Bladder Pain Syndrome (IC/BPS) and control subjects without a history of UTI or lower urinary tract symptoms [99–101]. Bladder infections prompt a rapid innate immune response, leading to a high level of IL-6 production [99, 102], which in turn facilitates inflammation and other acute phase responses [103, 104]. Additionally, Pre-SP, which is involved in transmitting pain signals to the central nervous system [105], has been found to induce secretion of TNF-α, IL-1β, and IL-6 in macrophages and monocytes [106–108]. Hence, these molecules play important roles in mediating innate immune defenses against bacterial infection [109–111]. Besides, the IHC (Figure S13) result demonstrated that the bacteria control group exhibited a significant increase in F4/80 protein expression (brown signals) compared to the no bacteria control group. In contrast, the TET and BSA-NDs groups demonstrated a decrease in F4/80 protein expression compared to the bacteria control group. The TET-BSA-NDs group displayed the most significant decrease in F4/80 protein expression among all the groups. This suggests that mice with bacterial infections treated with TET-BSA-NDs exhibited decreased F4/80 protein expression compared to TET and BSA-NDs alone, indicating that TET-BSA-NDs could potentially reduce the number of macrophages involved in the repair of bladder tissue after bacterial-induced injuries. Thus, TET-BSA-NDs represent a promising strategy to dampen macrophage-mediated inflammation in bacterial cystitis, offering advantages over conventional antibiotic therapy. This approach may inform targeted treatments for infections and inflammatory disorders, emphasizing the role of nanotechnology in optimizing drug delivery and immune modulation.

In addition to investigating the immune responses after the treatment with NDs, we also examined the proliferation of UPEC and the formation of IBC in umbrella cells on the urothelium layer of the bladder (Fig. 5E). After overnight treatment, the bladders of infected mice were dissected, and the urine and bacteria in the bladder lumen were washed away. The splayed bladders were then observed using fluorescence microscopy to identify the IBC (red dots representing bacterial aggregates). As shown in Fig. 5F, mice treated with TET-BSA-NDs showed the fewest bacterial aggregates signal compared to other treatments. To further confirm our result, we stained the bladders for LacZ expression in *E. coli* (Figure S14), in which IBC appeared as dark blue dots on the urothelium. These results strongly indicated that TET-BSA-NDs effectively entered the urothelium cells to kill the intracellular bacteria, resulting in enhanced antibacterial activity.

To quantify the amount of bacteria within the umbrella cells (IBC) of the urothelium layer, a CFU assay was conducted. After an overnight treatment, the bladders were collected from euthanized mice and treated with gentamicin to remove extracellular bacteria, which enabled counting IBC only. The bladders were subsequently prepared for the CFU assay. Following a serial dilution, the samples were placed on the LB agar plates with kanamycin, and the intracellular bacteria concentration (CFU/g of tissue) was determined by counting the number of colonies (Fig. 5G). As depicted in Fig. 5H, a 9.4% reduction was noted in the TET treatment group compared to the controls. Remarkably, a single dose of TET-BSA-NDs treatment has already eradicated nearly 90% of the IBC in urothelial cells in less than 24 h, suggesting that TET-BSA-NDs effectively halted IBC proliferation by delivering antibiotics into the bladder cells *via* NDs. Additionally, we quantified the bacteria in the lumen as a control and found that TET treatment significantly reduced bacteria by 75.8% in the infected bladder compared to the controls (Figure S15). Notably, TET-BSA-NDs treatment further decreased bacteria levels by an additional 34% compared to TET alone, demonstrating its potent antibacterial effectiveness. In addition to antibiotics, it is worth noting that the innate immune system also plays a crucial role in controlling and clearing intracellular infections, leading to the completely eradicating of bacterial infections [112–115]. Collaborative efforts of antimicrobial agents with immune cells, including monocytes [112] and neutrophils [116], or defense mechanisms, such as exfoliation of the infected urothelium [116–118], have been shown to clear intracellular bacteria successfully. Given that the initial number of IBC in the infected cells was dramatically alleviated after a single dosage of TET-BSA-NDs treatment, the immune system of the bladder cells can readily clear the IBCs without prolonged treatment or multiple dosing. Moreover, the highly efficient and effective killing effect of TET-BSA-NDs, which specifically reduces the number of IBC in a short period of time, followed by the host immune response for the clearance of bacteria, can further avoid the development of bacterial resistance. Existing studies

have demonstrated that the intravesical administration of nanoparticles containing chemotherapeutic drugs can effectively treat bladder cancers [119]. To the best of our knowledge, this is the first example of intravesical delivery of antibiotic-functionalized NDs to target UPEC in the infected bladder for UTI treatment.

Conclusion

In summary, we have successfully demonstrated the usage of antibiotic-functionalized NDs for the treatment of UTIs through intravesical delivery. We loaded tetracycline onto the BSA-NDs, and showed its excellent colloidal stability across various buffer systems. Moreover, the BSA-NDs act as the drug carriers to facilitate the entry of antibiotics in the cell, resulting in the improved antibacterial efficacy, reduced inflammatory responses, and enhanced intracellular bacterial clearance. Besides, importantly, our study introduced the technique of urethral catheterization for delivering antibiotic-loaded NDs for UTI treatment. This method effectively prevents the accumulation of NDs in organs, thereby minimizing potential toxic effects to the host. Additionally, it reduces the risk of drug loss during delivery, ensuring a sustained and effective drug concentration for optimal therapeutic effects. Although there is a risk of contamination in the process of urethral catheterization, the extreme hygiene setup and the safety precautions can effectively alleviate the potential complications of this practice. Ultimately, this approach can potentially be established as a standard framework for future ND-based drug delivery systems [61, 105].

Supplementary Information

The online version contains supplementary material available at https://doi.org/10.1186/s12951-025-03459-y.

Supplementary Material 1: The experimental section is available in Supporting Information. Supplementary data of mass characterizations, FT-IR spectra and fluorescence spectra of modified BSA molecules, DLS analysis, calibration curves of BSA and TET, release kinetics of TET-BSA-NDs in cell lysate, cytotoxicity of NDs, qPCR, LacZ staining are included in the Supporting Information.

Acknowledgements

Financial support was provided by Health and Medical Research Fund (TCKL: 20190932 and 22211142) and (PKL: 07181396, and 05160336), Hong Kong Research Grants Council (TCKL: 11102122) and (PKL: 11307421, 11301220, and 11304719), SKLMP Seed Collaborative Research Fund (PKL: SCRF/0040), The Science and Technology Innovation Committee of Shenzhen Municipality (PKL: JCYJ20190812160203619) and (KTC: JCYJ20210324133813036), City University of Hong Kong (TCKL: 7006039, 7020052 and 7005743), (PKL: 7005832, 9680104, and 7004911) and (KTC: 7005313, 7005518), the Croucher Foundation (KTC: 9509002 and 9500032) and Tung's Biomedical Sciences Centre (TCKL: 9609322 and 9609308) and (KTC: 9609306). The graphical abstract was created with BioRender.com.

Author contributions

C.O.K.L., H.M.L., and M.W. contributed equally. C.O.K.L., H.M. L., and M.W. performed experiments with the assistance from Q.N., Q.H.P., K.C.H., and T.S.W.; C.O.K.L., H.M.L., K.C.H., and T.S.W. analyzed the data. C.O.K.L., H.M.L., M.W., K.T.C., P.K.L., and T.C.K.L. wrote the manuscript. All authors agreed on the final version of the manuscript.

Data availability

No datasets were generated or analysed during the current study.

Declarations

Ethical approval

All experimental protocols were approved by the Animal Experimentation Ethics Committee of the City University of Hong Kong and Department of Health of Hong Kong Special Administrative Region (ref no. (21–240) in DH/HT&A/8/2/5 Pt.7) and in compliance with American Veterinary Medical Association guideline.

Consent for publication

All authors provide consent for the publication of the manuscript detailed above.

Competing interests

The authors declare no competing interests.

Author details

[1]Department of Biomedical Sciences and Tung Biomedical Sciences Centre, City University of Hong Kong, Kowloon, Hong Kong, SAR 999077, China
[2]Department of Chemistry and State Key Laboratory of Marine Pollution, City University of Hong Kong, Tat Chee Avenue, Kowloon, Hong Kong SAR 999077, China
[3]Biotech and Health Care, Shenzhen Research Institute of City University of Hong Kong, Shenzhen 518057, China
[4]Department of Pathology, Pamela Youde Nethersole Eastern Hospital, 3 Lok Man Road, Chai Wan, Kowloon, Hong Kong SAR 999077, China

Received: 6 February 2025 / Accepted: 11 May 2025
Published online: 21 May 2025

References

1. Sánchez SV, Navarro N, Catalán-Figueroa J, Morales JO. Nanoparticles as potential novel therapies for urinary tract infections. Front Cell Infect Microbiol. 2021;11:656496.
2. CDC. Urinary tract infection (catheter-associated urinary tract infection [CAUTI] and non-catheter-associated urinary tract infection [UTI]) events. 2023.
3. Newlands AF, Roberts L, Maxwell K, Kramer M, Price JL, Finlay KA. The recurrent urinary tract infection symptom scale: development and validation of a patient-reported outcome measure. BJUI Compass. 2023;4(3):285–97.
4. Yang X, Chen H, Zheng Y, Qu S, Wang H, Yi F. Disease burden and long-term trends of urinary tract infections: A worldwide report. Front Public Health. 2022;10.
5. Terlizzi ME, Gribaudo G, Maffei ME. UroPathogenic Escherichia coli (UPEC) infections: virulence factors, bladder responses, antibiotic, and non-antibiotic antimicrobial strategies. Front Microbiol. 2017;8:1566.
6. Kucheria R, Dasgupta P, Sacks S, Khan M, Sheerin N. Urinary tract infections: new insights into a common problem. Postgrad Med J. 2005;81(952):83.
7. Wang M, Wei H, Zhao Y, Shang L, Di L, Lyu C, et al. Analysis of multidrug-resistant bacteria in 3223 patients with hospital-acquired infections (HAI) from a tertiary general hospital in China. Bosnian J Basic Med Sci. 2019;19(1):86.
8. Klein RD, Hultgren SJ. Urinary tract infections: microbial pathogenesis, host–pathogen interactions and new treatment strategies. Nat Rev Microbiol. 2020;18(4):211–26.
9. Flores-Mireles AL, Walker JN, Caparon M, Hultgren SJ. Urinary tract infections: epidemiology, mechanisms of infection and treatment options. Nat Rev Microbiol. 2015;13(5):269–84.
10. Abraham SN, Miao Y. The nature of immune responses to urinary tract infections. Nat Rev Immunol. 2015;15(10):655–63.

11. Mulvey MA, Lopez-Boado YS, Wilson CL, Roth R, Parks WC, Heuser J, et al. Induction and evasion of host defenses by type 1-piliated uropathogenic Escherichia coli. Science. 1998;282(5393):1494–7.
12. Wright KJ, Seed PC, Hultgren SJ. Development of intracellular bacterial communities of uropathogenic Escherichia coli depends on type 1 pili. Cell Microbiol. 2007;9(9):2230–41.
13. Forbes R, Ali A, Abouhajar A, Brennand C, Brown H, Carnell S, et al. ALternatives to prophylactic antibiotics for the treatment of recurrent urinary tract infection in women (ALTAR): study protocol for a multicentre, pragmatic, patient-randomised, non-inferiority trial. Trials. 2018;19:1–19.
14. Albert X, Huertas I, Pereiro I, Sanfélix J, Gosalbes V, Perrotta C. Antibiotics for preventing recurrent urinary tract infection in non-pregnant women. Cochrane Database Syst Reviews. 2004(3).
15. Fisher H, Oluboyede Y, Chadwick T, Abdel-Fattah M, Brennand C, Fader M, et al. Continuous low-dose antibiotic prophylaxis for adults with repeated urinary tract infections (AnTIC): a randomised, open-label trial. Lancet Infect Dis. 2018;18(9):957–68.
16. Anselmo AC, Mitragotri S. Nanoparticles in the clinic: an update. Bioeng Translational Med. 2019;4(3):e10143.
17. Chauhan S, Jain N, Nagaich U. Nanodiamonds with powerful ability for drug delivery and biomedical applications: recent updates on in vivo study and patents. J Pharm Anal. 2020;10(1):1–12.
18. Kumari A, Kumar V, Yadav SK. Nanotechnology: a tool to enhance therapeutic values of natural plant products. Trends Med Res. 2012;7(2):34–42.
19. Patra JK, Das G, Fraceto LF, Campos EVR, Rodriguez-Torres MdP, Acosta-Torres LS, et al. Nano based drug delivery systems: recent developments and future prospects. J Nanobiotechnol. 2018;16(1):1–33.
20. Shinkai M, Yanase M, Suzuki M, Honda H, Wakabayashi T, Yoshida J, et al. Intracellular hyperthermia for cancer using magnetite cationic liposomes. J Magn Magn Mater. 1999;194(1–3):176–84.
21. Cui X, Pei R, Wang Z, Yang F, Ma Y, Dong S, et al. Layer-by-layer assembly of multilayer films composed of Avidin and biotin-labeled antibody for Immunosensing. Biosens Bioelectron. 2003;18(1):59–67.
22. Mah C, Zolotukhin I, Fraites TJ, Dobson J, Batich C, Byrne BJ. Microsphere-mediated delivery of Recombinant AAV vectors in vitro and in vivo. Mol Ther. 2000;1(5):S293.
23. Salata OV. Applications of nanoparticles in biology and medicine. J Nanobiotechnol. 2004;2(1):1–6.
24. Pantarotto D, Partidos CD, Hoebeke J, Brown F, Kramer ED, Briand J-P, et al. Immunization with peptide-functionalized carbon nanotubes enhances virus-specific neutralizing antibody responses. Chem Biol. 2003;10(10):961–6.
25. Nejabatdoust A, Zamani H, Salehzadeh A. Functionalization of ZnO nanoparticles by glutamic acid and conjugation with Thiosemicarbazide alters expression of efflux pump genes in multiple drug-resistant Staphylococcus aureus strains. Microb Drug Resist. 2019;25(7):966–74.
26. Rai MK, Deshmukh SD, Ingle AP, Gade AK. Silver nanoparticles: the powerful nanoweapon against multidrug-resistant bacteria. J Appl Microbiol. 2012;112(5):841–52.
27. Banoee M, Seif S, Nazari ZE, Jafari-Fesharaki P, Shahverdi HR, Moballegh A, et al. ZnO nanoparticles enhanced antibacterial activity of Ciprofloxacin against Staphylococcus aureus and Escherichia coli. J Biomedical Mater Res Part B: Appl Biomaterials. 2010;93(2):557–61.
28. Gu H, Ho PL, Tong E, Wang L, Xu B. Presenting Vancomycin on nanoparticles to enhance antimicrobial activities. Nano Lett. 2003;3(9):1261–3.
29. Sánchez-López E, Gomes D, Esteruelas G, Bonilla L, Lopez-Machado AL, Galindo R, et al. Metal-based nanoparticles as antimicrobial agents: an overview. Nanomaterials. 2020;10(2):292.
30. Dizaj SM, Lotfipour F, Barzegar-Jalali M, Zarrintan MH, Adibkia K. Antimicrobial activity of the metals and metal oxide nanoparticles. Mater Sci Engineering: C. 2014;44:278–84.
31. Malarkodi C, Rajeshkumar S. In vitro bactericidal activity of biosynthesized CuS nanoparticles against UTI-causing pathogens. Inorg Nano-Metal Chem. 2017;47(9):1290–7.
32. Mishra MP, Padhy RN. Antibacterial activity of green silver nanoparticles synthesized from Anogeissus acuminata against multidrug resistant urinary tract infecting bacteria in vitro and host-toxicity testing. J Appl Biomed. 2018;16(2):120–5.
33. Ahmad N, Ali S, Abbas M, Fazal H, Saqib S, Ali A, et al. Antimicrobial efficacy of Mentha piperata-derived biogenic zinc oxide nanoparticles against UTI-resistant pathogens. Sci Rep. 2023;13(1):14972.
34. Jing X, Park JH, Peters TM, Thorne PS. Toxicity of copper oxide nanoparticles in lung epithelial cells exposed at the air–liquid interface compared with in vivo assessment. Toxicol in Vitro. 2015;29(3):502–11.
35. McShan D, Ray PC, Yu H. Molecular toxicity mechanism of nanosilver. J Food Drug Anal. 2014;22(1):116–27.
36. Tortella GR, Rubilar O, Durán N, Diez MC, Martínez M, Parada J, et al. Silver nanoparticles: toxicity in model organisms as an overview of its hazard for human health and the environment. J Hazard Mater. 2020;390:121974.
37. Asharani PV, Wu YL, Gong Z, Valiyaveettil S. Toxicity of silver nanoparticles in zebrafish models. Nanotechnology. 2008;19(25):255102.
38. Jacobsen NR, Stoeger T, Van Den Brûle S, Saber AT, Beyerle A, Vietti G, et al. Acute and subacute pulmonary toxicity and mortality in mice after intratracheal instillation of ZnO nanoparticles in three laboratories. Food Chem Toxicol. 2015;85:84–95.
39. Shen T, Chernysheva MG, Badun GA, Popov AG, Egorov AV, Anuchina NM, et al. Levofloxacin and Amikacin adsorption on nanodiamonds: mechanism and application prospects. Colloids Interfaces. 2022;6(2):35.
40. Giammarco J, Mochalin VN, Haeckel J, Gogotsi Y. The adsorption of Tetracycline and Vancomycin onto nanodiamond with controlled release. J Colloid Interface Sci. 2016;468:253–61.
41. Wehling J, Dringen R, Zare RN, Maas M, Rezwan K. Bactericidal activity of partially oxidized nanodiamonds. ACS Nano. 2014;8(6):6475–83.
42. Iyer JK, Dickey A, Rouhani P, Kaul A, Govindaraju N, Singh RN, et al. Nanodiamonds facilitate killing of intracellular uropathogenic E. coli in an in vitro model of urinary tract infection pathogenesis. PLoS ONE. 2018;13(1):e0191020.
43. Barras A, Martin FA, Bande O, Baumann J-S, Ghigo J-M, Boukherroub R, et al. Glycan-functionalized diamond nanoparticles as potent E. coli anti-adhesives. Nanoscale. 2013;5(6):2307–16.
44. Turcheniuk V, Raks V, Issa R, Cooper IR, Cragg PJ, Jijie R, et al. Antimicrobial activity of menthol modified nanodiamond particles. Diam Relat Mater. 2015;57:2–8.
45. Rouhani P, Singh RN. Polyethyleneimine-functionalized magnetic Fe3O4 and nanodiamond particles as a platform for amoxicillin delivery. J Nanosci Nanotechnol. 2020;20(7):3957–70.
46. Lee D-K, Kim SV, Limansubroto AN, Yen A, Soundia A, Wang C-Y, et al. Nanodiamond–gutta percha composite biomaterials for root Canal therapy. ACS Nano. 2015;9(11):11490–501.
47. Lee D-K, Kee T, Liang Z, Hsiou D, Miya D, Wu B, et al. Clinical validation of a nanodiamond-embedded thermoplastic biomaterial. Proc Natl Acad Sci. 2017;114(45):E9445–54.
48. Wang D, Tong Y, Li Y, Tian Z, Cao R, Yang B. PEGylated nanodiamond for chemotherapeutic drug delivery. Diam Relat Mater. 2013;36:26–34.
49. Gwak R, Lee G-J, Kim H, Lee M-K, Rhee C-K, Dae-Ro C, et al. Efficient doxorubicin delivery using deaggregated and carboxylated nanodiamonds for cancer cell therapy. Nanosci Nanatechnol Lett. 2015;7(9):723–8.
50. Norouzi N, Ong Y, Damle VG, Najafi MBH, Schirhagl R. Effect of medium and aggregation on antibacterial activity of nanodiamonds. Mater Sci Engineering: C. 2020;112:110930.
51. Chang BM, Lin HH, Su LJ, Lin WD, Lin RJ, Tzeng YK, et al. Highly fluorescent nanodiamonds protein-functionalized for cell labeling and targeting. Adv Funct Mater. 2013;23(46):5737–45.
52. Tzeng YK, Faklaris O, Chang BM, Kuo Y, Hsu JH, Chang HC. Superresolution imaging of albumin-conjugated fluorescent nanodiamonds in cells by stimulated emission depletion. Angew Chem Int Ed. 2011;50(10):2262–5.
53. Leung HM, Lau CH, Ho JW-T, Chan MS, Chang TJH, Law LH, et al. Targeted brain tumor imaging by using discrete biopolymer-coated nanodiamonds across the blood–brain barrier. Nanoscale. 2021;13(5):3184–93.
54. Kulshrestha P, Giese RF, Aga DS. Investigating the molecular interactions of Oxytetracycline in clay and organic matter: insights on factors affecting its mobility in soil. Environ Sci Technol. 2004;38(15):4097–105.
55. Chan MS, Liu LS, Leung HM, Lo PK. Cancer-cell-specific mitochondria-targeted drug delivery by dual-ligand-functionalized nanodiamonds circumvent drug resistance. ACS Appl Mater Interfaces. 2017;9(13):11780–9.
56. Li R, Vedelaar TA, Sigaeva A, Zhang Y, Wu K, Wang H, et al. Fluorescent nanodiamonds for tracking single polymer particles in cells and tissues. Anal Chem. 2023;95(35):13046–54.
57. Zhang Y, Sharmin R, Sigaeva A, Klijn CWM, Mzyk A, Schirhagl R. Not all cells are created equal – endosomal escape in fluorescent nanodiamonds in different cells. Nanoscale. 2021;13(31):13294–300.

58. Prabhakar N, Khan MH, Peurla M, Chang H-C, Hänninen PE, Rosenholm JM. Intracellular trafficking of fluorescent nanodiamonds and regulation of their cellular toxicity. ACS Omega. 2017;2(6):2689–93.
59. Casey JR, Grinstein S, Orlowski J. Sensors and regulators of intracellular pH. Nat Rev Mol Cell Biol. 2010;11(1):50–61.
60. Wurpel DJ, Totsika M, Allsopp LP, Hartley-Tassell LE, Day CJ, Peters KM, et al. F9 fimbriae of uropathogenic Escherichia coli are expressed at low temperature and recognise Galβ1-3GlcNAc-containing glycans. PLoS ONE. 2014;9(3):e93177.
61. Welch RA, Burland V, Plunkett G III, Redford P, Roesch P, Rasko D, et al. Extensive mosaic structure revealed by the complete genome sequence of uropathogenic Escherichia coli. Proc Natl Acad Sci. 2002;99(26):17020–4.
62. Subramaniam S, Joyce P, Ogunniyi AD, Dube A, Sampson SL, Lehr C-M, et al. Minimum information for conducting and reporting in vitro intracellular infection assays. ACS Infect Dis. 2024;10(2):337–49.
63. Meier C, Oelschlaeger TA, Merkert H, Korhonen TK, Hacker J. Ability of the newborn meningitis isolate Escherichia coli IHE3034 (O18: K1: H7) to invade epithelial and endothelial cells. Infect Immun. 1996;64:2391–9.
64. Tulkens PM. Intracellular distribution and activity of antibiotics. Eur J Clin Microbiol Infect Dis. 1991;10:100–6.
65. Hardie J, Makabenta JM, Gupta A, Huang R, Cao-Milán R, Goswami R, et al. Selective treatment of intracellular bacterial infections using host cell-targeted bioorthogonal nanozymes. Mater Horiz. 2022;9(5):1489–94.
66. Jiang L, Greene MK, Insua JL, Pessoa JS, Small DM, Smyth P, et al. Clearance of intracellular Klebsiella pneumoniae infection using gentamicin-loaded nanoparticles. J Controlled Release. 2018;279:316–25.
67. Qi H, Shan P, Wang Y, Li P, Wang K, Yang L. Nanomedicines for the efficient treatment of intracellular bacteria: the ART principle. Front Chem. 2021;9:775682.
68. Röhrig C, Huemer M, Lorgé D, Luterbacher S, Phothaworn P, Schefer C, et al. Targeting hidden pathogens: cell-penetrating enzybiotics eradicate intracellular drug-resistant Staphylococcus aureus. MBio. 2020;11(2):10–1128.
69. Huemer M, Mairpady Shambat S, Brugger SD, Zinkernagel AS. Antibiotic resistance and persistence—Implications for human health and treatment perspectives. EMBO Rep. 2020;21(12):e51034.
70. Haddad Kashani H, Schmelcher M, Sabzalipoor H, Seyed Hosseini E, Moniri R. Recombinant endolysins as potential therapeutics against antibiotic-resistant Staphylococcus aureus: current status of research and novel delivery strategies. Clin Microbiol Rev. 2018;31(1):10–1128.
71. Schmelcher M, Donovan DM, Loessner MJ. Bacteriophage endolysins as novel antimicrobials. Future Microbiol. 2012;7(10):1147–71.
72. Bongers S, Hellebrekers P, Leenen LPH, Koenderman L, Hietbrink F. Intracellular penetration and effects of antibiotics on Staphylococcus aureus inside human neutrophils: a comprehensive review. Antibiotics. 2019;8(2):54.
73. Qiu Y, Hou Y, Sun F, Chen P, Wang D, Mu H, et al. Hyaluronic acid conjugation facilitates clearance of intracellular bacterial infections by streptomycin with neglectable nephrotoxicity. Glycobiology. 2017;27(9):861–7.
74. Pearson JC, Gillett E, Gadri ND, Dionne B. Tetracyclines, the old and the new: A narrative review. CMI Commun. 2025;2(1):105059.
75. Musher DM, Minuth JN, Thorsteinsson SB, Holmes T. Effectiveness of achievable urinary concentrations of tetracyclines against Tetracyclne-Reslstant pathogenic Bacteria. J Infect Dis. 1975;131(Supplement):S40–4.
76. Rosenstock J, Smith LP, Gurney M, Lee K, Weinberg WG, Longfield JN, et al. Comparison of single-dose Tetracycline hydrochloride to conventional therapy of urinary tract infections. Antimicrob Agents Chemother. 1985;27(4):652–4.
77. Agwuh KN, MacGowan A. Pharmacokinetics and pharmacodynamics of the tetracyclines including glycylcyclines. J Antimicrob Chemother. 2006;58(2):256–65.
78. Mawabo IK, Noumedem JAK, Kuiate JR, Kuete V. Tetracycline improved the efficiency of other antimicrobials against gram-negative multidrug-resistant bacteria. J Infect Public Health. 2015;8(3):226–33.
79. Olajuyigbe OO. Synergistic influence of Tetracycline on the antibacterial activities of amoxicillin against resistant bacteria. J Pharm Allied Health Sci. 2012;2(1):12–20.
80. He Y, Zhao W, Dong Z, Ji Y, Li M, Hao Y, et al. A biodegradable antibacterial alginate/carboxymethyl Chitosan/Kangfuxin sponges for promoting blood coagulation and full-thickness wound healing. Int J Biol Macromol. 2021;167:182–92.
81. Hao Y, Zheng W, Sun Z, Zhang D, Sui K, Shen P, et al. Marine polysaccharide-based composite hydrogels containing fucoidan: preparation, physicochemical characterization, and biocompatible evaluation. Int J Biol Macromol. 2021;183:1978–86.
82. Leung HM, Liu LS, Cai Y, Li X, Huang Y, Chu HC, et al. Light-Activated Nanodiamond-Based drug delivery systems for Spatiotemporal release of antisense oligonucleotides. Bioconjug Chem. 2024;35(5):623–32.
83. Chu L, Gao H, Cheng T, Zhang Y, Liu J, Huang F, et al. A charge-adaptive nanosystem for prolonged and enhanced in vivo antibiotic delivery. Chem Commun. 2016;52(37):6265–8.
84. Radovic-Moreno AF, Lu TK, Puscasu VA, Yoon CJ, Langer R, Farokhzad OC. Surface Charge-Switching polymeric nanoparticles for bacterial cell Wall-Targeted delivery of antibiotics. ACS Nano. 2012;6(5):4279–87.
85. Rahuman HBH, Dhandapani R, Palanivel V, Thangavelu S, Paramasivam R, Muthupandian S. Bioengineered phytomolecules-capped silver nanoparticles using Carissa carandas leaf extract to embed on to urinary catheter to combat UTI pathogens. PLoS ONE. 2021;16(9):e0256748.
86. Whelan S, Lucey B, Finn K. Uropathogenic Escherichia coli (UPEC)-Associated urinary tract infections: the molecular basis for challenges to effective treatment. Microorganisms [Internet]. 2023;11(9).
87. Rosen DA, Hooton TM, Stamm WE, Humphrey PA, Hultgren SJ. Detection of intracellular bacterial communities in human urinary tract infection. PLoS Med. 2007;4(12):e329.
88. Klumpp David J, Rycyk Matthew T, Chen Michael C, Thumbikat P, Sengupta S, Schaeffer Anthony J. Uropathogenic Escherichia coli induces extrinsic and intrinsic cascades to initiate urothelial apoptosis. Infect Immun. 2006;74(9):5106–13.
89. Wu Y, Weil T. Nanodiamonds for biological applications. Phys Sci Reviews. 2017;2(6).
90. Yuan Y, Chen Y, Liu J-H, Wang H, Liu Y. Biodistribution and fate of nanodiamonds in vivo. Diam Relat Mater. 2009;18(1):95–100.
91. Miao C, Zhang Y, Liu G, Yang J, Yu K, Lv J, et al. Multi-step strategies for synergistic treatment of urinary tract infections based on D-xylose-decorated antimicrobial peptide carbon Dots. Biomaterials. 2024;308:122547.
92. Chen L, Deng H, Cui H, Fang J, Zuo Z, Deng J, et al. Inflammatory responses and inflammation-associated diseases in organs. Oncotarget. 2018;9(6):7204.
93. Murray PJ. Macrophage polarization. Annu Rev Physiol. 2017;79(1):541–66.
94. McNab F, Mayer-Barber K, Sher A, Wack A, O'Garra A. Type I interferons in infectious disease. Nat Rev Immunol. 2015;15(2):87–103.
95. Kawai T, Akira S. Toll-like receptors and their crosstalk with other innate receptors in infection and immunity. Immunity. 2011;34(5):637–50.
96. Griffith JW, Sokol CL, Luster AD. Chemokines and chemokine receptors: positioning cells for host defense and immunity. Annu Rev Immunol. 2014;32(1):659–702.
97. Ricciotti E, FitzGerald GA. Prostaglandins and inflammation. Arterioscler Thromb Vasc Biol. 2011;31(5):986–1000.
98. Van Lint P, Libert C. Chemokine and cytokine processing by matrix metalloproteinases and its effect on leukocyte migration and inflammation. J Leucocyte Biology. 2007;82(6):1375–81.
99. Jiang Y-H, Peng C-H, Liu H-T, Kuo H-C. Increased pro-inflammatory cytokines, C-reactive protein and nerve growth factor expressions in serum of patients with interstitial cystitis/bladder pain syndrome. PLoS ONE. 2013;8(10):e76779.
100. Martins SM, Darlin DJ, Lad PM, Zimmern PE. Interleukin-1B: a clinically relevant urinary marker. J Urol. 1994;151(5):1198–201.
101. March CJ, Mosley B, Larsen A, Cerretti DP, Braedt G, Price V, et al. Cloning, sequence and expression of two distinct human interleukin-1 complementary DNAs. Nature. 1985;315(6021):641–7.
102. Nielubowicz GR, Mobley HLT. Host–pathogen interactions in urinary tract infection. Nat Reviews Urol. 2010;7(8):430–41.
103. Wei X, Li B, Wu L, Yin X, Zhong X, Li Y, et al. Interleukin-6 gets involved in response to bacterial infection and promotes antibody production in nile tilapia (Oreochromis niloticus). Dev Comp Immunol. 2018;89:141–51.
104. Tanaka T, Narazaki M, Kishimoto T. IL-6 in inflammation, immunity, and disease. Cold Spring Harb Perspect Biol. 2014;6(10):a016295.
105. Cao YQ, Mantyh PW, Carlson EJ, Gillespie A-M, Epstein CJ, Basbaum AI. Primary afferent tachykinins are required to experience moderate to intense pain. Nature. 1998;392(6674):390–4.
106. Cuesta MC, Quintero L, Pons H, Suarez-Roca H. Substance P and calcitonin gene-related peptide increase IL-1β, IL-6 and TNFα secretion from human peripheral blood mononuclear cells. Neurochem Int. 2002;40(4):301–6.
107. Rameshwar P, Ganea D, Gascon P. In vitro stimulatory effect of substance P on hematopoiesis. 1993.

108. Lotz M, Vaughan JH, Carson DA. Effect of neuropeptides on production of inflammatory cytokines by human monocytes. Science. 1988;241(4870):1218–21.
109. Li X, Körner H, Liu X. Susceptibility to intracellular infections: contributions of TNF to immune defense. Front Microbiol. 2020;11:1643.
110. Febriza A, Natzir R, Hatta M, As'ad S, Budu B, Kaelan C, et al. The role of IL-6, TNF-α, and VDR in inhibiting the growth of *Salmonella typhi*: In vivo study. Open Microbiol J. 2020;14:65–71.
111. Slaats J, Ten Oever J, van de Veerdonk FL, Netea MG. IL-1β/IL-6/CRP and IL-18/ferritin: distinct inflammatory programs in infections. PLoS Pathog. 2016;12(12):e1005973.
112. Li J, Claudi B, Fanous J, Chicherova N, Cianfanelli FR, Campbell RAA, et al. Tissue compartmentalization enables Salmonella persistence during chemotherapy. Proc Natl Acad Sci. 2021;118(51):e2113951118.
113. Zurawski DV, McLendon MK. Monoclonal antibodies as an antibacterial approach against bacterial pathogens. Antibiot [Internet]. 2020;9(4).
114. Handel A, Margolis E, Levin BR. Exploring the role of the immune response in preventing antibiotic resistance. J Theor Biol. 2009;256(4):655–62.
115. Pankey GA, Sabath LD. Clinical relevance of bacteriostatic versus bactericidal mechanisms of action in the treatment of Gram-Positive bacterial infections. Clin Infect Dis. 2004;38(6):864–70.
116. Mulvey MA, Schilling JD, Martinez JJ, Hultgren SJ. Bad bugs and beleaguered bladders: Interplay between uropathogenic *Escherichia coli* and innate host defenses. Proc Natl Acad Sci U S A. 2000;97(16):8829–35.
117. Mctaggart LA, Rigby RC, Elliott TSJ. The pathogenesis of urinary tract infections associated with Escherichia coli, Staphylococcus Saprophyticus and S. Epidermidis. J Med Microbiol. 1990;32(2):135–41.
118. Fukushi Y, Orikasa S, Kagayama M. An electron microscopic study of the interaction between vesical epitherlium and E. Coli Invest Urol. 1979;17(1):61–8.
119. Kates M, Date A, Yoshida T, Afzal U, Kanvinde P, Babu T, et al. Preclinical evaluation of intravesical cisplatin nanoparticles for non–muscle-invasive bladder cancer. Clin Cancer Res. 2017;23(21):6592–601.

Publisher's note